Nuclear Materials Authority
P.O.Box 530 Maadi, Cairo, Egypt

ISSN 2314-5609
Nuclear Sciences Scientific Journal
9A, 63- 84
2020
http://www.ssnma.com

RADIOACTIVITY, PETROGENESIS AND RARE EARTH ELEMENTS TETRAD EFFECT OF THE MINERALIZED GRANITE OF GABAL GATTAR, NORTH EASTERN DESERT, EGYPT

EHAB K. ABU ZEID
Nuclear Materials Authority, Cairo, Egypt

ABSTRACT

The batholith of Gabal Gattar is bounded by diorite and granodiorite from the northeastern corner and Hammamat sediments from the northwestern corner. Wadi Belih extends between Hammamat sediments and Gabal Gattar following a major fault trending N75°-80°E. Petrographically, the studied Gattarian granites at GII occurrence composed mainly of potash feldspar, plagioclase and quartz associated with substantial percentage of mica minerals. Modal composition revealed that this granite is quartz-rich syenogranite. Microscopic examination clarifies the presence of two types of secondary radioactive minerals; the first type is syngenetic comprising the minerals that derived from the primary minerals (uraninite-coffinite) as uranophane and kasolite associating the metamict zircon and violet fluorite. The second type of the secondary uranium minerals is epigenetic like uranophane which is the most common secondary uranium mineral that formed by hydrothermal solutions using the silica ions that derived from the silicate minerals. Radioactivity of the studied granite is very high where eU varies between 450 and 4600 ppm with an average 1889.7 ppm, eTh between 0.59 and 900 ppm with an average 80 ppm, Ra between 418 and 2530 ppm with an average 1212 ppm and potassium between 0.01 and 2.40 % with an average 1.05%. The binary relations between the radionuclides show that uranium mineralization in GII occurrence are mainly connected to hydrothermal alteration processes during the late stages of magmatic crystallizations. The ratios (La/Y and Y/Ho)and the anomalies (Ce-and Eu-), in addition to the recorded pattern of REEs tetrad effect (M-type) for the studied granite indicate that this granite is highly evolved and affected by late stage hydrothermal alteration. Mineralogical investigations clarified that U-minerals comprise the primary minerals (uraninite and pitchblende) and the secondary minerals (uranophane and kasolite).

INTRODUCTION

Gattar granites were investigated by Schurman (1966), El-Shazly (1970), El-Rakaiby and Shalaby (1992), Nossier (1996) and El-Kammar et al. (2001). Gabal (G.) Gattar batholith is located in the North Eastern Desert of Egypt between Lat. 26° 52' N and 27° 08' N and Long. 33° 13' E and 33° 26' E west of Hurghada town by 50 Km (Fig. 1). The granite of Gabal Gattar is a good hostile for uranium mineralization and pays attention for advanced studies. The prospecting project of the Nuclear Materials Authority (NMA) includes 21 occurrences, published in El-Kholy et al. (2019) according to the date of discovery, G-I, G-II, G-III,..etc. All of them are located in the northwestern part of the batholith (Fig. 1).

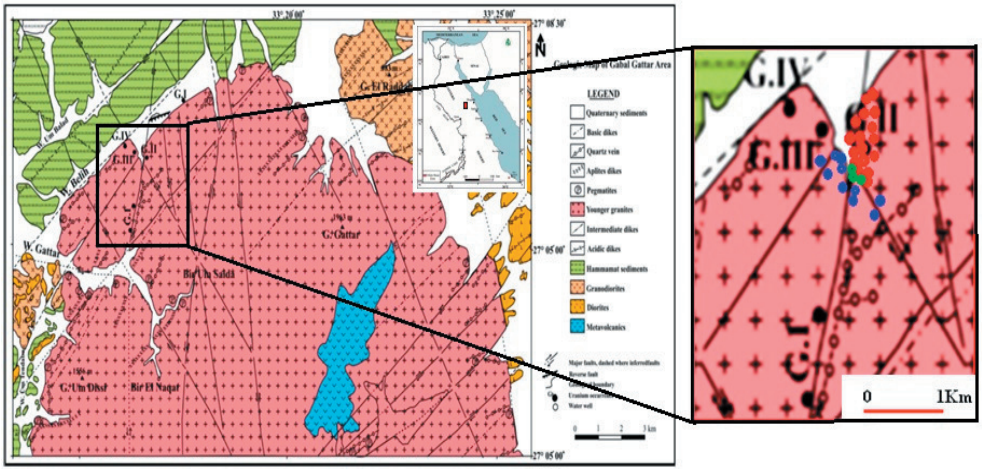

Samples of GII occurrence, Samples of surrounding rocks, Samples used for tetrad effect

Fig. 1 : Geological map of Gabal Gattar area (After Roz, 1994)

Uranium occurrence of G-II represents a good target for prospecting due to its high potentiality of uranium where recent surface exploration activities have led to the discovery of new promising uranium mineralized zones on the surface of this occurrence. Visible secondary uranium mineralization of bright yellow and orange colors, were recorded on the various levels of the exposures. The uranium mineralization extends along a highly sheared, silicified and hematitized zones; following NNE-SSW and NW-SE trends; the mineralization increase at the intersection zones of these trends.

Roz (1994) studied the geology of G. Gattar and reported that it is mainly composed of younger granite which forms marginal sharp intrusive contacts with the surrounding country-rocks that include; metavolcanics, diorite and Hammamat sediments.

Darwish (1999) studied the petrographic characteristics of the episyenitized granite of G. Gattar granites and concluded that the mineralized granites were affected by different types of hydrothermal fluids of different compositions and temperatures that played an important role in providing, mobilizing and concentrating of uranium.

Attawiya et al. (1999) studied the geochemical characteristics of G. Gattar granite and concluded that the younger granite of G. Gattar is alkali feldspar granite originated from a peraluminous calc-alkaline magma with some alkaline affinities and emplaced in within plate magmatic (anorogenic) tectonic setting. They referred to the silica depletion in some varieties where the quartz and feldspars dissolved by hydrothermal solution through a process of episyenitization and concluded that the episyenitized granite of G. Gattar is characterized by high levels of radioactivity.

El-Kaliouby et al. (2003) stated that Gattar granite is two-feldspars and two-mica granite containing primary muscovite and biotite minerals and belonging to S-type granite generated by anatexis of crustal rocks.

Mahdy et al. (2014) studied the radioactivity of G. Gattar and concluded that fluorite is synchronous with the uranium mineralization, providing evidence that the source of the uranium is the host granite and the uranium transported as uranium–fluoride complexes. The fluorine is the essential factor for mobilization

and enrichment of uranium in the late stage magmatic residual fluids through fractional crystallization and then hydrothermal solutions. The uranium-rich granite underwent tectono-hydrothermal processes causing alterations of rock forming minerals. The mineralizing solutions may be uranium bearing of hypogene and supergene origin percolating through the granites and leached uranium. Then, mobilization of uranium within the granite, and deposition of uranium and fluorite mineralization along fractures provided easy channels for the passage of uranium–fluorine bearing solutions and later as suitable structural traps for uranium-fluorite deposition.

Shalaby et al. (2015) explained that the muscovite of Gattar granite is secondary formed by metamorphic/metasomatic processes, with crystallization temperature between 300 and 400 °C. It is considered as late to post-magmatic mineral phases generated from hydrothermally altered granitic rocks and concluded that Gattar granite is A-type granite. They reported two types of structurally controlled ores in Gattar granite; the uranium-fluorite and molybdenum-bismuth-silver ores, and the two kinds of ore have different trending and isolated occurrence to form single deposits for the same host Gattar granite.

The study aims to shed light on the radioactive potentiality of the granite of GII-occurrence clarifying the uranium minerals responsible for this radioactivity and pointing to their genesis and geochemical features controlling the redistribution of rare earth elements.

METHODOLOGY

Twenty seven representative samples were collected from the mineralized granites representing the highest values of anomalous field radioactivity. These samples were prepared for gamma-ray spectrometric analysis in order to determine their uranium, thorium, radium and potassium contents by using multichannel analyzer (MCA) of gamma-ray detector (Gamma-Spectrometer technique). The instrument used in determination of the four radioactive elements consists of a Bicron scintillation detector NaI (Tl) 76x76 mm, hermetically sealed with the photomultiplier tube in aluminum housing. The tube is protected by a copper cylinder protection of thickness 0.6 cm against induced X ray and a chamber of lead bricks against environmental radiation. Uranium, thorium, radium and potassium are measured by using four energy regions representing Th^{234}, Pb^{212}, Pb^{214} and K^{40} at 93 kV, 239 kV, 352 kV and 1460 kV for uranium, thorium, radium and potassium, respectively. The measurements were carried out in sample plastic containers, cylindrical in shape, 212.6 cm^3 volumes with 9.5 cm average diameter and 3 cm height. The rock sample is crushed to about 1 mm grain size and then the container is filled with about 300-400 gm of the crushed sample sealed well and left for at least 21days to accumulate free radon to attain radioactive equilibrium. The relation between the percentage of Rn^{222} accumulation and time increases till reaching the steady stage after about 38 days, (Matolin, 1991).

For mineralogical investigation, the representative sample was properly crushed, ground and sieved before subjecting the liberated size fractions to heavy minerals separation using bromoform (Sp. Gr. = 2.85 gm/cm^3). From the obtained heavy fractions, pure mineral grains were handpicked and investigated under the binocular microscope. Some of the picked mineral grains were subjected to analysis by X-ray diffraction analysis using PHILIPS X-ray diffractometer (model PW 3710/31) and Environmental Scanning Electron Microscope (ESEM). This instrument is supported by an energy dispersive spectrometer unit (EDS) model PHILIPS XL-30. The applied analytical conditions involved 30 kV as the accelerating voltage, 1-2 µm beam diameter during 60 to 120 seconds as counting time and the minimum detectable weight concentration ranging from 0.1 to 1% .

The thin sections were studied using plane polarized microscope (model OLYMPUS BX53) attached with digital camera. A thin polished section examined by reflected polarized light to distinguish the kasolite and to establish the reflectivity of kasolite compared with the uranophane.

Three samples of the mineralized granite were analyzed for Y and rare earth elements by ICP emission spectrometry (ICP-ES). Radiometric measurements, mineralogical studies and chemical analyses were carried out in NMA laboratories.

GEOLOGIC OUTLINES

The pluton of G. Gattar bounded by diorite and granodiorite from the northeastern corner and Hammamat sediments from the northwestern corner. Wadi (W.) Belih extends between Hammamat sediments and G. Gattar following a major fault trending N75°-80°E, more or less parallel to the local reverse fault separating these sediments from the intruded granites to the south (Salman et al., 1986 and Shalaby, 1996). Wadi Gattar and its tributaries located in the western side of the pluton trending WNW (Fig. 1).

Exploratory mine and development work indicated that the uranium mineralizations continuously extend from the surface to a depth at least 40 m. The uranium mineralizations are associated with several processes of hydrothermal alteration (silicification, hematitization, kaolinitization, muscovitization, albitization) associated with pyrite and fluorite. The degree of alteration, especially hematitization and silicification, increases with the high concentration of mineralization and considered as good targets for study. The primary uranium mineralizations concentrated in closely spaced fracture zones, following NNE-SSW and NW-SE trends, intersections of fractures are the most favorable sites for mineralizations

The pitchblende of greyish black color occurs in thin smears along minor fractures as well as squeezed in the microfractures of the sheared parts. Its occurrence is sporadic as irregular lenticular with strike of N35°E and dipping to SE with dip angle of 55°.

The uranium mineralization is usually found associated with gangue minerals, commonly represented by quartz, fluorite and carbonates. Secondary generated quartz and uranium mineralization show an intimate intergrowth in microfractures. In some parts, the amorphous silica coating the mineralized surface, and may protect them from alteration.

PETROGRAPHY

Microscopic examination for the thin sections of eight samples from G. Gattar syeno-

Table 1: Modal analysis (%) for the mineralogical composition of the mineralized syenogranite of G. Gattar (GII)

Sample No.	Quartz	Potash feldspar	Plagioclase	Mafic minerals	Opaques & Accessories
EG9	38.3	39.7	15.6	2.7	3.7
EG10	41.1	37.3	14.3	2.8	4.5
EG12	37.9	42.1	11.7	3.1	5.2
EG13	39.8	39.6	13.2	2.6	4.8
EG14	39.2	37.1	16.9	3.2	3.6
EG15	40.7	36.5	14.5	1.8	6.5
EG16	38.1	38.5	17.1	2.5	3.8
EG17	38.6	41.0	13.4	1.9	5.1
Av.	**39.2**	**39.0**	**14.6**	**2.6**	**4.7**

granite confirmed its mineralogical composition as potash feldspar, plagioclase and quartz. Modal analysis of this rock (Table 1) revealed that it is quartz-rich granite and the potash feldspar is more dominant rather than the plagioclase. Graphical presentation for the modal analyses of these rocks using the ternary diagram of Streckeisen, (1976) located the samples in the field of syenogranite (Fig. 2)

Feldspar minerals, represented by plagioclase and potash feldspars, are the main constituents for this rock (> 52%). Potash feldspar minerals are the most susceptible minerals to hematization; they appear as euhedral crystals of string perthite mostly characterized by nodules of iron oxides (Fig. 3). Plagioclase (An_{12-14}) is less common that present as euhedral crystals of oligoclase exhibiting its characteristic lamellar twining; they are partially saussuritized (Fig. 4). Quartz is relatively high occupying about 39.2% of the rock occurring as primary anhedral crystals coagulated in clusters (Fig. 5) exhibiting its characteristic wavy extinction and first-order grey interference color and as secondary fine crystals produced by silicification of the feldspars (3-4% of the total quartz). It is the most susceptible mineral

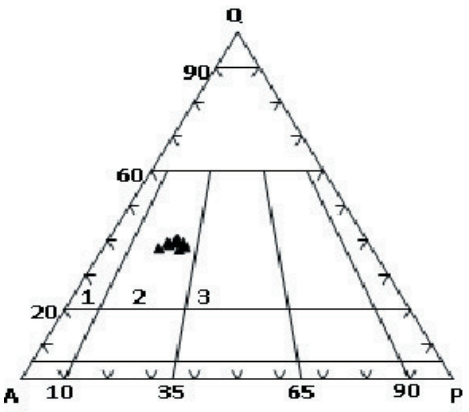

Fig. 2: Modal analysis of Gabal Gattar (GII) syenogranite (According to Streckeisen, 1976)
Fields: 1=Alkali feldspar granite, 2= Syenogranite, 3=Monzogranite

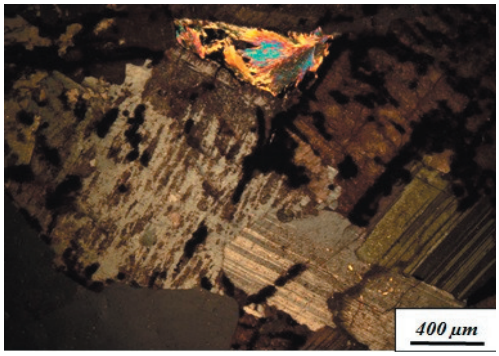

Fig. 3: Photomicrograph of GII-syenogranite showing euhedral crystals of perthite, plagioclase and quartz with fan-shaped muscovite, XPL

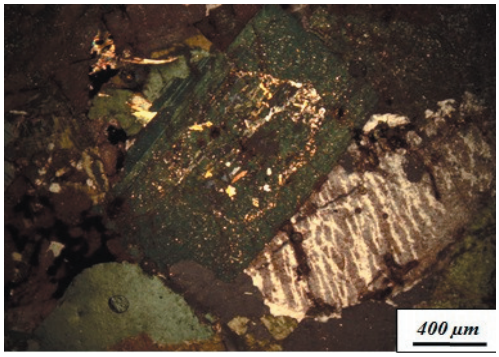

Fig. 4: Photomicrograph of GII-syenogranite showing euhedral crystal of partially saussiritized plagioclase associating string perthite, XPL

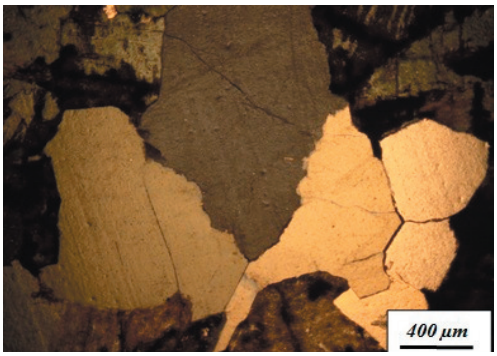

Fig. 5: Photomicrograph of GII-syenogranite showing coagulation of quartz associating the feldspars, XPL

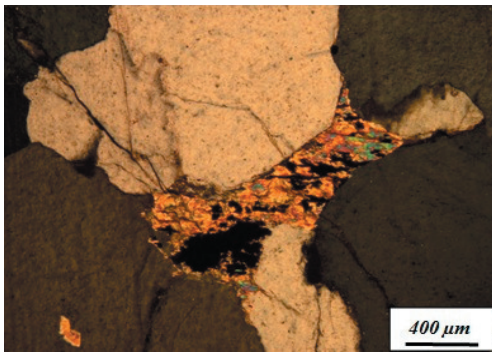

Fig. 6: Photomicrograph of GII-syenogranite showing anhedral crystal of quartz partially replaced by secondary uranium-mineral, XPL

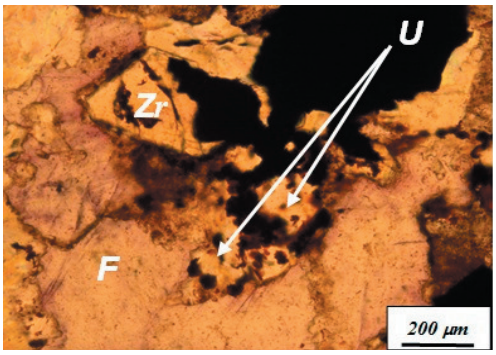

Fig. 7: Photomicrograph of GII-syenogranite showing well-formed zircon (*Zr*) associated with uranophane (*U*) and violet fluorite (*F*), PPL

to the process of dissolving and replacement by the action of hydrothermal solution (Fig. 6). Mica minerals occupy about 2.6% of the rock represented by muscovite that present as secondary interstitial fine flakes of fan-shaped muscovite (Fig. 3) or as minute flakes formed by muscovitization of the feldspars by hydrothermal solutions. Most of the rock-forming minerals are stained with iron oxides which occasionally adsorb uranium causing intense uranium mineralization.

Accessory minerals represented mainly by zircon beside fluorite and the radioactive minerals (Fig. 7). Zircon appears as well-formed crystals with yellow color and faint isotropism losing its interference colors and tightly associated with uranophane and fluorite (Fig. 8). Fluorite occurs as coarse crystals with violet color and isotropic character (Fig. 9). Khazback et al., (1995) attributed variation in colors of fluorite in Gattar granite to disturbance in its crystal lattice as result of radiogenic effect of the associated uranium minerals. There are several accessory minerals that previously recorded such as monazite, apatite and allanite

The present study interested in the uranium-minerals; microscopic examination revealed presence of two types of the secondary radioactive minerals. The first types syn-

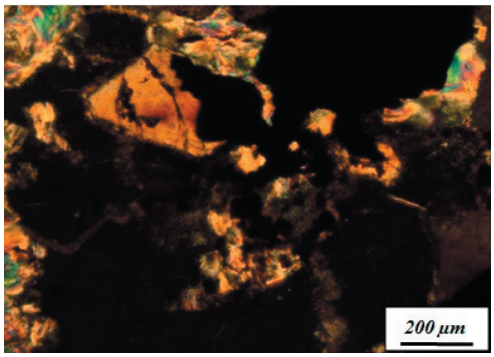

Fig. 8: Corresponding view for well-formed zircon associated with uranophane and fluorite, XPL

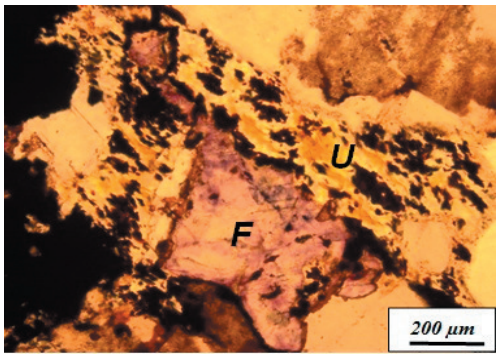

Fig. 9: Photomicrograph of GII-syenogranite showing overgrowth of syngenetic uranophane (*U*) associating violet fluorite (*F*), PPL

genetic comprising the minerals that derived from the primary minerals (uraninite-coffinite) in the magma. They are found firmly associating the proper heavy minerals, where uranophane accompanies the metamict zircon and violet fluorite based on the defect structure of fluorite that occupied by U-ions (Fig. 8). Kasolite is another secondary uranium mineral found as transparent patches with orange color and weak pleochroism associating uranophane as lead-rich hydrated alteration for uraninite (Figs. 10&11). Examination of thin-polished section revealed presence of speaks with moderate reflectivity as relics of galena associating the kasolite that characterized by yellow internal reflection, (Fig. 12).

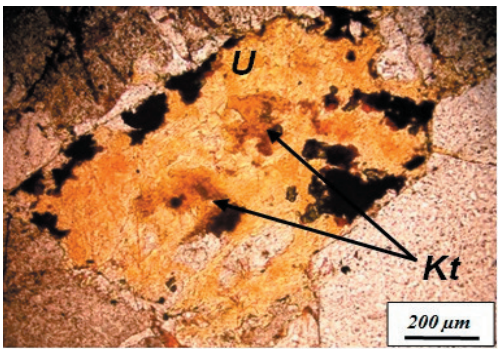

Fig. 10: Photomicrograph of GII-syenogranite showing orange patches of kasolite (*Kt*) accompanying amorphous uranophane (*U*), PPL

Three postulations may be proposed for the secondary syngenetic radioactive minerals; the first in the silica-poor magma where the uranous ions (U^{4+}) of uraninite combine with the other trace elements such as the lead and few silica forming kasolite [$Pb(UO_2)(SiO_4 \cdot H_2O$]. The second in the silica-rich magma where the uranous ions (U^{4+}) combine completely with the silicate and crystallize as coffinite [$U(SiO_4)_{1x}(OH)_{4x}$] that transformed to uranophane [$Ca(UO_2)2SiO_3(OH)_{2.5}(H_2O)$]. The third postulation, in the evolved magma, where the uraninite evolved to coffinite and the two corresponding syngentic secondary minerals (kasolite and uranophane) would be formed stimulating the event of mineralized granite of G. Gattar. Thus, the two secondary minerals are derived from- and genetically related to the primary uraninite of the magma proved by presence of kasolite (low silica) accompanying the uranophane (silica-rich), (Fig. 10).

The second type of the secondary uranium minerals is epigenetic comprising the minerals that formed post magmatic where the uranous

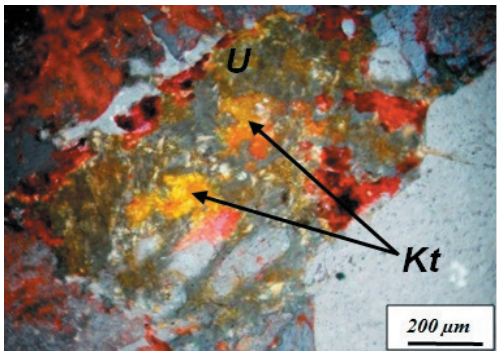

Fig. 11: Photomicrograph of GII-syenogranite showing corresponding view for kasolite (*Kt*) accompanying amorphous uranophane (*U*), XPL

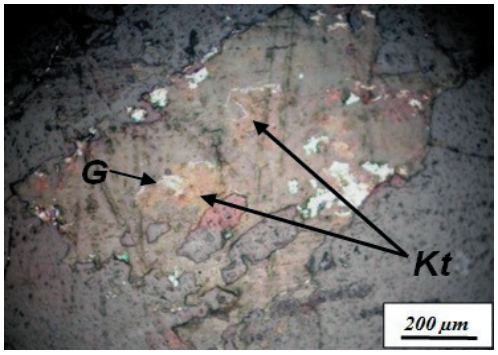

Fig. 12: Photomicrograph of GII-syenogranite showing corresponding polished section of kasolite (*Kt*) and uranophane with relics of galena (*G*), RL

ions (U^{4+}), derived from distal uranium-rich source, oxidized to uranyl ions (U^{6+}) that soluble in the hydrothermal solutions. They moved and reprecipitated when reduced in presence of reducing agent. The process of replacement is an epigenetic process where the hydrothermal minerals dissolve the essential minerals (feldspars and quartz) replacing them by iron oxides and secondary uranium minerals. Uranophane is the most common secondary uranium mineral that formed by hydrothermal solutions using the silica ions that derived from the silicate minerals; where the microscopic examination clarified that it replaces quartz (Figs. 13&14), perthite (Fig. 15) and plagioclase (Fig. 16).

Fig. 14: Photomicrograph of GII-syenogranite showing epigenetic uranophane with relics of quartz, XPL

RADIOACTIVITY

Twenty seven samples from uranium-mineralized granite at GII uranium occurrence selected and measured by Na-I detector for determination of radionuclide concentrations beside three samples used for tetrad effect. The radioactive minerals that responsible for anomaly of the studied granite examined by the electron scanning environmental microscope (ESEM) to throw light on their chemical composition by EDX analysis.

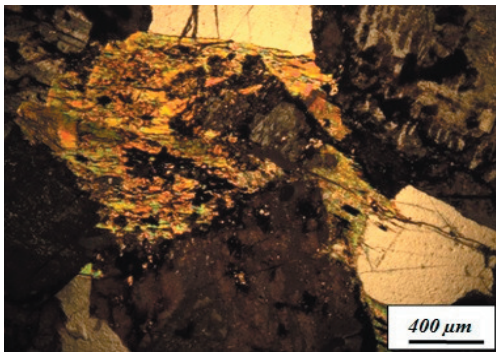

Fig. 15: Photomicrograph of GII-syenogranite showing epigenetic uranophane replacing perthite, XPL

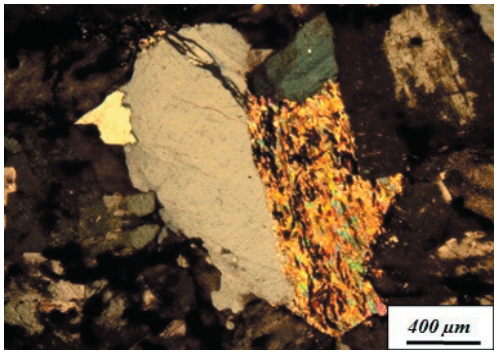

Fig. 13: Photomicrograph of GII-syenogranite showing epigenetic uranophane partially replacing quartz, XPL

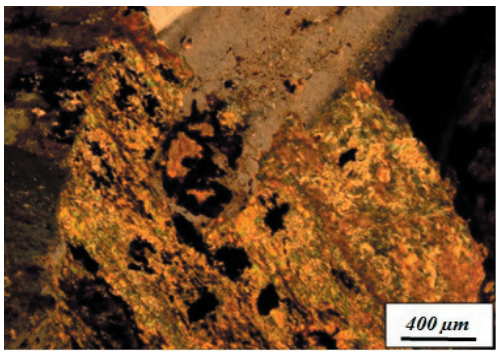

Fig. 16: Photomicrograph of GII-syenogranite showing epigenetic uranophane partially replacing plagioclase, XPL

Radiometric Measurements

The equivalent uranium contents in the studied samples varied between 450 and 4600 ppm with 1889.74 ppm as an average, eTh between 0.59 and 900 ppm and averaging 80 ppm, RaeU between 418 and 2530 ppm with an average 1212 ppm while potassium between 0.01 and 2.40 % with a mean of 1.05%.

Uraniferous granites are radiometrically characterized by high contents of U (>8 ppm) and/or Th (>16 ppm) with or without U-mineralization (Darnely 1982). This may be manifested that Gattar granites could be considered as mineralized granites where they contain about nineteen folders of uraniferous granites contents. The mineralized character of Gattar granites was also confirmed from eTh/eU and eU/eTh ratios. The eU/eTh ratio is an important radiometric parameter to identify the sites of U-mineralization. It is used also to detect the oxidation state in which U transported (Naumov, 1959). The productive uraniferous rocks have U/Th ratio >1 (Darnely and Ford, 1989; Raslan and El-Feky, 2012). The investigated rocks have eU/eTh ratio values ranging between 3.61 and 4269.66 with an average of 1138.58. (Table 2). This means that, Gattar granites are considered as productive uraniferous rocks, (Darnely, 1982 and Naumov, 1959).

Table 2: Radiometric measurements and ratios for the studied mineralized G. Gattar granites at GII- occurrence

Sample No.	eU (ppm)	eTh (ppm)	Ra (ppm)	K (%)	eTh/eU	eU/eTh	eU/Ra
G1	2300	22	1136	0.01	0.0096	104.55	2.02
G 2	1310	1.5	820	0.55	0.0011	873.33	1.60
G3	3800	0.89	1120	0.7	0.0002	4269.66	3.39
G4	3458	0.84	1339	0.9	0.0002	4116.67	2.58
G5	1910	1.01	1040	0.88	0.0005	1891.09	1.84
G6	3500	0.99	1510	1.08	0.0003	3535.35	2.32
G7	2101	0.94	1100	0.09	0.0004	2235.11	1.91
G8	4600	1.08	1700	0.04	0.0002	4259.26	2.71
G9	760	25	627	0.94	0.0329	30.40	1.21
G10	690	1.2	614	1.11	0.0017	575.00	1.12
G11	1390	1.54	960	1.7	0.0011	902.60	1.45
G12	980	70	750	1.4	0.0714	14.00	1.31
G13	714	30	685	1.2	0.0420	23.80	1.04
G14	660	0.89	759	1.56	0.0013	741.57	0.87
G15	450	1.08	418	1.25	0.0024	416.67	1.08
G16	560	1.09	480	1.22	0.0019	513.76	1.17
G17	481	1.70	705	1.76	0.0035	282.94	0.68
G18	2400	0.59	1900	1.9	0.0002	4067.80	1.26
G19	1400	30	980	1.24	0.0214	46.67	1.43
G20	899	1.33	881	1.1	0.0015	675.94	1.02
G21	1480	1.45	1180	2.4	0.0010	1020.69	1.25
G22	2840	50	2170	0.22	0.0176	56.80	1.31
G23	2454	110	1949	0.77	0.0448	22.31	1.26
G24	3250	900	2530	0.98	0.2769	3.61	1.28
G25	3040	780	2480	0.87	0.2566	3.90	1.23
G26	1746	55	1370	1.4	0.0315	31.75	1.27
G27	1850	70	1540	1.2	0.0378	26.43	1.20
Av.	**1889.74**	**80.00**	**1212.70**	**1.05**	**0.03**	**1138.58**	**1.51**
Min.	**450.00**	**0.59**	**418.00**	**0.01**	**0.00**	**3.61**	**0.68**
Max.	**4600.00**	**900.00**	**2530.00**	**2.40**	**0.28**	**4269.66**	**3.39**

Uranium is fixed under reducing conditions, where it has an insoluble tetravalent state and converted to the soluble hexavalent state which could be mobilized into solution but thorium has a single insoluble tetravalent state which is geochemically associated with uranium and, therefore, is a useful standard for comparison purposes (Doventon and Prensky, 1992). eU-eTh cross plot (Fig. 17) indicates irregular correlation between these elements suggesting oxidation of uranium and its mobilization away its associating elements resulting U-rich mineralizing solutions which is confirmed by very high eU/eTh ratios. eU-eTh/eU and eTh-eTh/eU binary diagrams also indicate irregular relation referring to the role of post-magmatic hydrothermal solutions in redistribution of these elements (Figs. 18&19).

Potassium content affected by two opposite processes; kaolinization that increases the K% and sericitization that liberate potassium ions and escaping from the rock causing disturbance in the relations**.** The potassium–thorium diagram could be considered as indication clay mineral associations and the characterization of micas and feldspars (Macfarlane et al., 1989). As both thorium (by adsorption) and potassium (chemical composition) are associated with clay minerals, the ratio eTh/K expresses relative potassium enrichment as

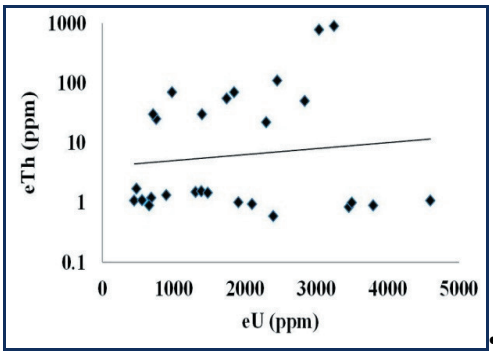

Fig. 17: eU-eTh variation diagram of GII-syenogranite

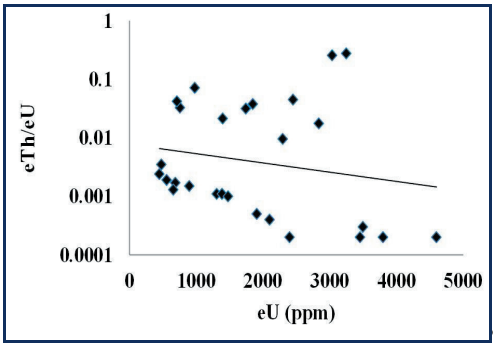

Fig. 18: eU-eTh/eU ratio variation diagram of GII-syenogranite

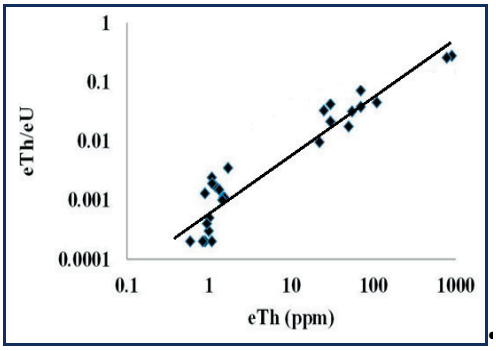

Fig. 19: eTh-eTh/eU ratio variation diagram of GII- syenogranite

an indicator of clay-mineral species, and as might be diagnostic of other radioactive minerals (Anjos et al., 2005). This means that the positive correlation may be related to clay mineral formation resulted from alteration processes and alkali metasomatism, or combined to magmatic differentiation processes. The irregular relations between eU-K and eTh-K, suggests the mobilization of uranium and thorium escaping apart of potassium and/or each other (Figs. 20&21).

eU-Ra binary diagram and eU/Ra ratio clarify positive disequilibrium in most samples suggesting uranium accumulation resulting from recent uranium deposits (Fig.22). The negative disequilibrium in

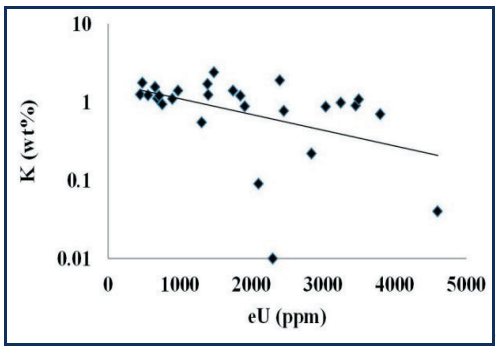

Fig. 20: eU-K variation diagram of GII-syenogranite

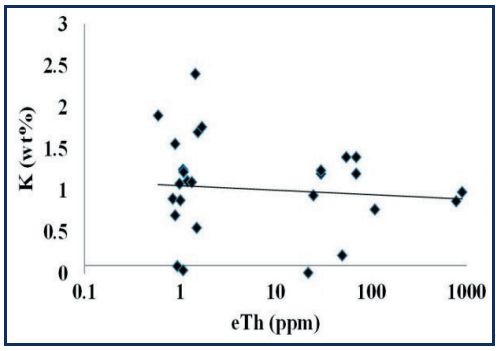

Fig. 21: eTh-K variation diagram of GII-syenogranite

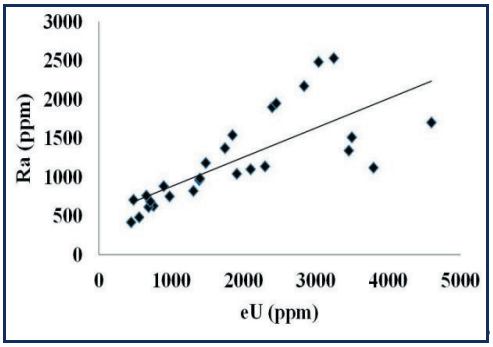

Fig. 22: eU-Ra variation diagram of GII-syenogranite

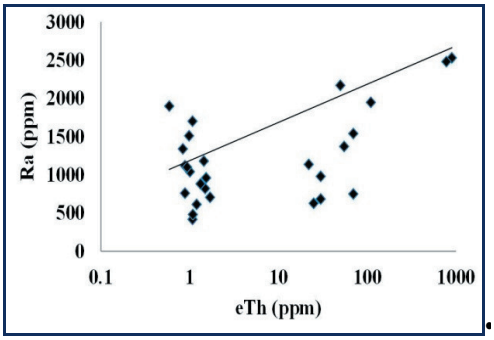

Fig. 23: eTh-Ra variation diagram of GII-syenogranite

some samples (Table 2) may manifest uranium leaching processes due to acidic alteration processes as kaolinization or silicification or radon escaping in the sheared parts, on the other hand the relation eTh-Ra is irregular (Fig. 23).

RADIOACTIVE MINERALS

The thin sections examined by electron scanning environmental microscope (ESEM) to study the radioactive minerals that responsible for the anomaly of GII-occurrence. They could be distinguished to primary U-minerals (uraninite and pitchblende) and secondary U-minerals (uranophane and kasolite).

Primary U-minerals

They were recognized in GII-granite as uraninite and pitchblende; and their composition clarified as follows:

Uraninite(UO_2)

Uraninite is the crystalline mineral of UO_2 present as cubic crystals with brownish black color and submetallic luster. Five spot analyses were carried out along the intercept of uraninite grains by (ESEM), (Fig. 24). EDX analysis indicated that the uraninite of GII occurrence is considered as a HRRE-enriched uraninite (Fig.24). The high contents of Pb

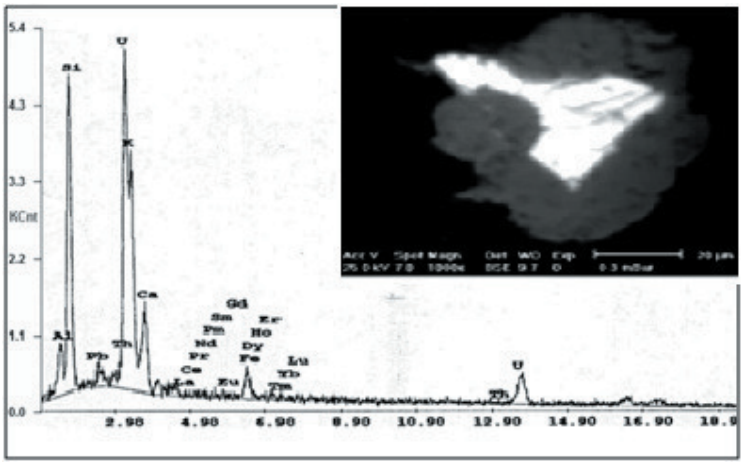

Fig. 24: ESEM spectrograph and BSE image for uraninite from GII-syenogranite

and the nearly obscure Th in the studied uraninite may indicate a typical vein type deposits (Snelling, 1980). The grains of the mineral separated and identified by XRD; the diffractogram illustrated on Figure (25).

Pitchblende (UO_2)

Pitchblende is a non-crystalline variety of uraninite that occurs chiefly in low-temperature (T <250 ^oC) (Frondel, 1958 and Nash et al., 1981). Microscopically, it is present as aggregate of amorphous black mineraloid with botryoidal form. The composition of the separated grains recognized by EDX analysis indicating presence of uranium as the main constituent associated with radiogenic lead. Four analyses by ESEM were conducted along the intercept of pitchblende grain showing its spectrograph (Fig. 26) and images for the colloformal texture (Fig. 26a) and botroyids (Fig. 26b).

Secondary U-minerals

In the present study, the secondary U-minerals recognized as uranophane and kasolite**.**

Uranophane ($Ca(UO_2)_2SiO_3(OH)_{2.5}(H_2O)$)

Uranophane present as films, patches, crusts or aggregate of needle-like crystals of monoclinic system. It is a uranyl silicate mineral fairly common in the oxidized zone of most deposits (Cebron et.al., 1993). It occurs syngenetically as alteration of uraninite containing black and/or brown inclusions mainly from fluorite and iron oxides and epigenetically by hydrothermal solution. Five spot analyses by (ESEM) were carried out for uranophane grain (Fig. 27)

The conditions for the formation of secondary uranyl silicates have been investigated by Korzeb et al. (1997). These conditions include both the late stages reactions of uraninite with hydrothermal solutions and also alteration by ground water. Rismsaite (1982) noted that uranium released during the alteration of pitchblende in the oxidation zone forms several generations of secondary uranium minerals. The earlier generation being enriched in lead, (e.g. kasolite and masuyite) whiles the later one impoverished in lead, (e.g. uranophane).

The lead content of uranophane is low in comparison with uraninite and pitchblende suggesting its younger age (Osmond et al., 1999). He reported that there was an episode of uranium migration and secondary mineral

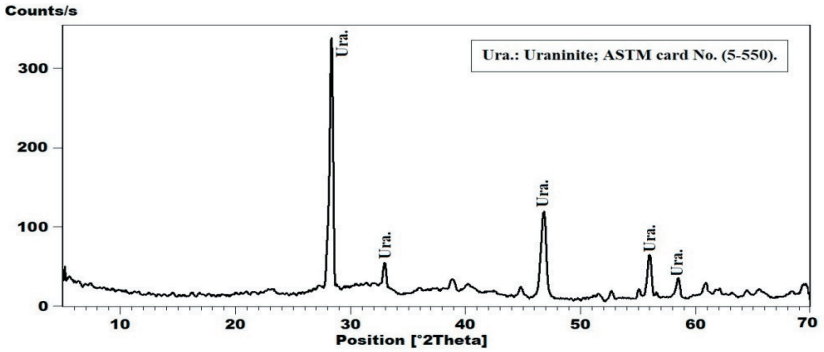

Fig. 25: XRD diffractogram of uraninite mineral

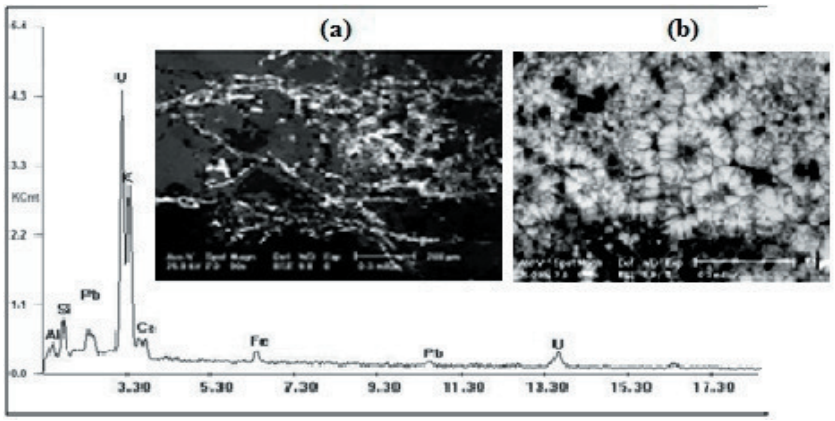

Fig. 26: ESEM spectrograph and BSE image of (a) pitchblende with colloform texture and (b) botroyids of pitchblende from GII-syenogranite

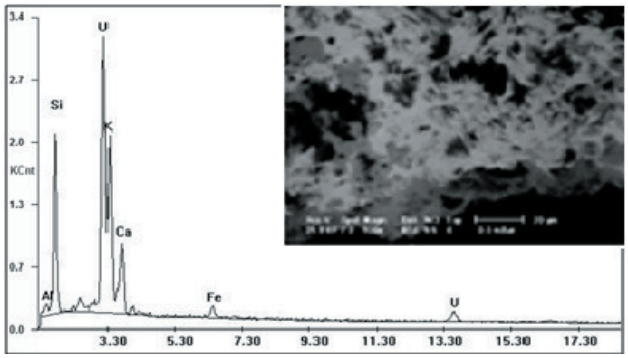

Fig. 27: ESEM spectrograph and BSE image for uranophane from GII-syenogranite

formation in the eastern desert of Egypt (ca. 100,000 year). This age is coincident with Pluvial periods in Egypt, during which the Eastern Desert was flooded by surface water. Ibrahim et al. (2001) concluded that during the Pluvial periods, the underground water level is raised and consequently it can also play a role in formation of secondary uranium under suitable conditions of temperature and pH.

Kasolite $Pb(UO_2)(SiO_4) \cdot H_2O$

Kasolite is the hydrated oxide mineral of lead uranyle. It is present as aggregate of needle-like crystals of monoclinic system. This mineral is secondary syngenetic mineral found associating the syngenetic uranophane as patches of orange color in the studied granite (GII-locality), (Fig. 10). BSE image clarified that kasolite associated with galena (Fig. 28) and its spectrograph confirmed its composition clarifying uranium, lead and silica as the main constituents (Fig. 28), while those of galena are mainly lead and sulfur (Fig. 29).

Burns and Finch (1999) stated that the associating galena originated from the radiogenic lead from uraninite decay in presence of reducing agent according to his equation:

$$(U^{4+}U^{6+}PB^{2+})O_2+HS(1-Y)\longrightarrow UO_2+YPBS+YOH+1/2YO_2$$

He added that Pb combines with UO_2^{2+} under oxidizing conditions where the pb-uranyle oxyhydroxides commonly form directly from precursor uraninite to form one or more of the 25 known Pb-uranyle minerals and their genesis is probably related to the accumulation of radiogenic lead. Hazen et al. (2009) suggested a process of auto-oxidation that caused by radioactive decay and the formation of helium from alpha particles; then, he predicted a mixture of several uranyle minerals including soddyite, curite and kasolite.

REEs AND SOME PETROGENETIC ASPECTS

The behavior of REEs and radioelements in granites is mainly controlled by the solubility of accessory minerals in the melt (Montel, 1986). Three samples (S9, S9a and S9b) picked from an anomalous shearing zone and

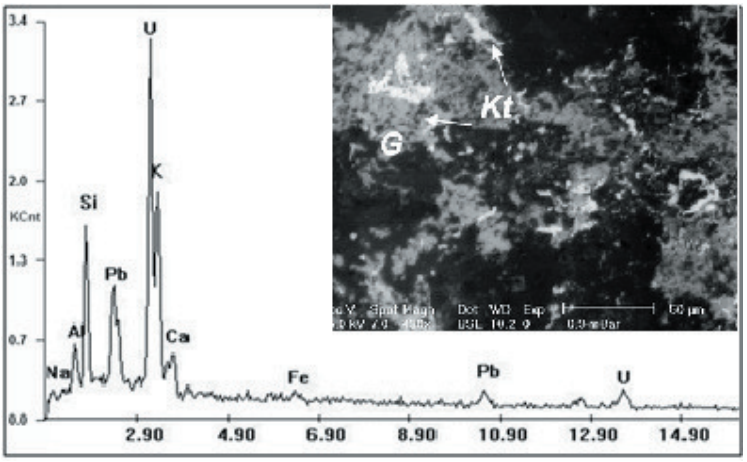

Fig. 28: ESEM spectrograph and BSE image for kasolite (Kt) surrounded by galena (G) from GII-syenogranite

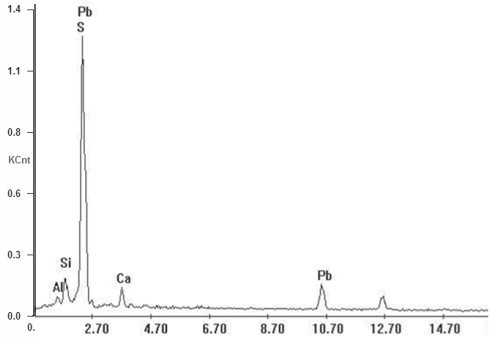

Fig. 29: ESEM spectrograph of galena from GII-syenogranite

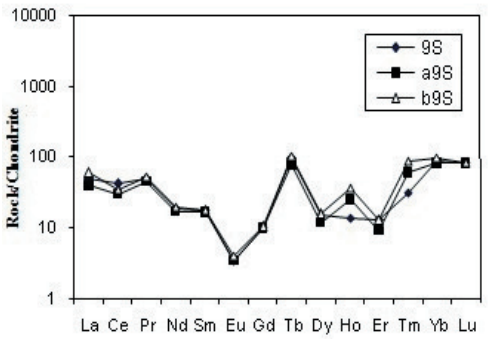

Fig. 30: Chondrite-normalized REEs pattern for selected samples of GII-granite (According to Boynton, 1984)

analyzed for determination of REEs concentrations (Fig. 30) that used in calculations for the tetrad effect (Table 3). The distribution of REE between minerals is highly controlled by magmatic and metamorphic processes as well as subsequent alteration (Möller et al., 1994). Gramaccioli and Segolstad (1978) stated that monazite may contain significant amounts of radioelements in its structure and considered as the principal Th-ore and a major REEs ore. The high contents of REEs and radioelements may indicate that monazite is slightly affected by hydrothermal fluids invading the host granite rocks. Belousova et al. (1998) stated that solid solution of xenotime with zircon introduces large amounts of Y and HREEs into the zircon structure.

The average of the total REEs content of the studied silicified granite (av. ΣREE= 121.99 ppm) which is lower than that of the world-wide granite (ΣREE=250-270 ppm) as reported by Herman (1970). The REEs depletion is mainly revised to various processes as magmatic differentiation (Cuney and Friedrich, 1987), hydrothermal leaching (Cathelineau, and Holliger, 1987) and or a combination of both (Ibrahim and Darwish, 2012).

The LREEs average (75.83 ppm) of the studied mineralized granites is higher than the average of HREEs (46.17 ppm). $(La/Yb)_{cn}$ ratios average of Gattar granites (0.36) clarify the abundance of HREEs. The HREEs enrichment could confirm the highly fractionated nature of the studied granites.

Y/Ho Ratio

Fractionation between some isovalent pairs of trace elements such as Y-Ho which show geochemically similar behavior (Gadd et al., 2016) can yield useful information about evolution history of deposits. Geochemically, these pairs are controlled by their radius and charge (CHARAC) in geological environments (Bau, 1996). This means that the Y/Ho ratio can reflect the physicochemical conditions of the depositional environment. The chondritic value (Y/Ho = 28.8) is recorded for samples didn't affected by hydrothermal alteration where deviation of Y/Ho ratio from the chondritic values is only related to samples showing a tetrad effect (Zhang et al., 1994). The studied samples have Y/Ho ratios lower than the Chondritic value, one sample has chondritic ratio (sample S9), (Table 4). The complexation with fluorine is interpreted as major cause for Y/Ho>28, while the complexation with bicarbonate is assumed to generate Y/Ho values <28, suggesting that the solution causing tetrad effect is mainly complexed with carbonates which confirmed by the presence of calcite and malachite in the studied mineralized granites.

Table 3: REEs analyses and geochemical parameters for anomalous samples of Gattar granite (GII)

REE	Sample No.			
	S9	S9a	S9b	Av.
La	18.2	14.5	21.8	18.2
Ce	39.5	28.33	33.0	33.6
Pr	6.7	6.18	7.22	6.7
Nd	13.1	12.1	14	13.1
Sm	4.0	3.8	4.1	4.0
Eu	0.3	0.3	0.35	0.32
Gd	3.1	3.0	3.2	3.0
Tb	5.5	4.5	6.0	5.3
Dy	5.8	4.5	5.97	5.4
Ho	1.18	2.11	3.13	2.14
Er	3.22	2.25	3.19	2.9
Tm	1.12	2.14	3.09	2.1
Yb	22	20	24	22
Lu	3.2	3.1	3.2	3.2
Y	33.3	35	34.5	34.3
REEs geochemical parameters				
• *REEs*	126.92	106.81	132.25	122
LREEs	81.8	65.21	80.47	75.83
HREEs	45.12	41.6	51.78	46.16
La/Y	0.55	0.41	0.63	0.53
Y/Ho	28.22	16.59	11.02	18.61
*Eu/Eu**	0.70	0.80	0.80	0.76
Ce/Ce'	1.158	0.992	0.839	0.996
$(La/Yb)_{cn}$	0.4	0.3	0.4	0.36
$La/Sm)_{cn}$	1.8	1.5	2.1	1.8

Table 4: Geochemical parameters used for REEs tetrad effect for selected samples of GII-granite

Sample No.	S9	S9a	S9b
t1	1.49	1.41	1.25
t3	3.21	1.94	2.06
t4	1.6	2.57	2.79
TE1..3	2.18	1.66	1.60
TE1..4	1.54	1.90	1.87

La/Y Ratio

La/Y ratio values >1 and <1 are related to alkalic and acidic environment, respectively (Maksimovic and Pantó, 1996). So, La/Y could be used as a criterion to indicate the acidic and/or alkalic conditions of the depositional environment. All samples of the studied mineralized granites have La/Y ratio values (<1), indicating that the mineralizing solution is mainly acidic. This may suggest that these acidic solutions have high ability for solubilizing uranium and REEs-bearing minerals which may be precipitated due to pH changes by the presence of alkaline carbonate solutions as indicated from Y/Ho ratio (Sallam et al., 2020).

Ce Anomaly

Cerium is an oxidation-sensitive element; Ce-anomaly is strongly controlled by the fugacity of oxygen during geochemical processes. Increasing oxygen fugacity in an environment causes Ce^{3+} to become oxidized to Ce^{4+} which has a smaller ionic radius and greater charge. Studies have shown that Ce^{4+} in most geological environments is less mobile (Kraemer et al., 2017). Ce-anomalies (<1) were likely formed in reducing conditions and those with the values >1 formed in oxidation conditions. Ce-anomalies in the studied mineralized granite samples are higher and lesser than the unity suggesting changes in the physicochemical conditions during leaching and precipitation of uranium and the other associating elements.

Eu Anomaly

Europium is also an oxidation-sensitive element which has two oxidation states, Eu^{2+} and Eu^{3+}, during geochemical processes. As clarified in SHAB theory (Qicong and Congqiang, 2010), low oxygen fugacity (almost reducing) environments, Eu^{2+}, along with soft bases such as HS^-, S^{2-} and CH_4 are commonly formed. Thus, Eu^{2+} can form more stable complexes and precipitate from solutions or fluids after being oxidized to Eu^{3+} (Tang et al., 2013). Decomposition of Eu-bearing miner-

als (feldspars) during hydrothermal activities can release Eu into solutions/fluids which is strongly mobile, and reduction of Eu^{3+} to Eu^{2+} can occur at temperatures >200ºC (Schwinn and Markl, 2005). The presence of negative Eu- anomalies in the studied samples indicate that the mineralizing solutions, having temperature >200ºC, low pH, and relatively low $fO2$, facilitating the alteration of Gattar granites.

REE Tetrad Effect

The term 'tetrad effect' in geochemistry refers to the subdivision of the 15 lanthanide elements into four groups in a chondrite normalized distribution pattern: (1) La–Ce–Pr–Nd, (2) Pm–Sm–Eu– Gd, (3) Tb–Dy–Ho, and (4) Er–Tm–Yb–Lu, and each group forms a smooth convex (M-type) or concave (W-type) pattern (Masuda et al., 1987). The values of tetrad effect were calculated according to the quantification method of Irber (1999):

$$T1 = (CE/CE^{*} \times PR/PR^{*}),\ T3 = (TB/TB^{*} \times DY/DY^{*}),\ T4 = (TM/TM^{*} \times YB/YB^{*})$$

Degree of the tetrad effect $T1,3 = (t1 \times t3)^{0.5}$.

The REE pattern that does not show a tetrad effect has values of $TE_{1.3} < 1.1$. The M-shaped pattern shows TEi > 1.1 and the W-shaped TEi < 0.9.

The M-shaped tetrad effect has been reported from most granites and igneous systems in which crystallization and fluid-rock interactions were suggested to be the main mechanisms for producing the tetrad effect (McLennan, 1994 and Nardi et al., 2012). The kinks in the REE patterns are camouflaged by prominent convex tetrads and pronounced negative Eu anomalies. The REE-tetrad effect patterns of the studied samples indicated that the third tetrad is more prominent than the first and fourth tetrad where the second tetrad isn't characterized resulting from the anomalous behavior of europium. The REE patterns also manifested that the presence of strong tetrads from the third and fourth type relative the first one. The indices of tetrad effect intensity, TE1,3 and TE1,4, are higher than 1.10 ranging from 1.6 to 2.18 and1.54 to 1.9, respectively, suggesting interaction between melt and water-haloids-rich fluid when these granites are crystallized from magma (El-Mezayen et al., 2019).

CONCLUSIONS

GII uranium occurrence is an anomalous site that described as mineralized granite occupying Part of the northwestern corner of G. Gattar and representing one of the most important U-occurrences in the area. The area dissected by several Shear zones and the granite could be categorized microscopically as uraniferous syenogranite due to presence of the U-minerals and dominance of potash feldspars rather than the plagioclase.

Radiometric measurements recorded anomalous readings for uranium potentiality (up to 4600ppm) and the binary relations between each couple of radionuclides indicated obvious disturbance referring to the effect of late- to post-magmatic processes of hydrothermal alteration and U-enrichment. On the other hand, these processes played an important role in redistribution of the rare earth elements that expressed as M-type pattern of tetrad effect. The kinks in the REE patterns are camouflaged by prominent convex tetrads and pronounced negative Eu anomalies. The REE-tetrad effect patterns of the studied samples indicated that the third tetrad is more prominent than the first and fourth tetrad where the second tetrad isn't characterized resulting from the anomalous behavior of europium. The indices of tetrad effect intensity, TE1,3 and TE1,4, are higher than 1.10 ranging from 1.6 to 2.18 and 1.54 to 1.9, respectively, suggesting interaction between melt and water-haloids-rich fluid when these granites are crystallized from magma. The ratios (La/Y and Y/Ho) and the anomalies (Ce-and Eu-), in addition to the recorded pattern of REEs tetrad effect (M-type) for the studied granite indicate that this granite is highly evolved and affected by late stage hydrothermal alteration.

Microscopic investigations revealed presence of secondary U-minerals as uranophane and kasolite, while ESEM examinations confirmed presence of primary minerals as uraninite and pitcheblende. The study reached to presence of two types of the secondary U-minerals; the first is syngenetic that formed in magma directly from the primary minerals by hydration, oxidation or/and confusion with the silicate giving to kasolite and uranophane. The reality of this idea proved by permanent tight association with magmatic accessory minerals (zircon, fluorite and galena) and presence of radiogeneic lead in kasolite that derived from uraninite. The second type of the secondary U-minerals is epigenetic that formed post-magmatic by hydrothermal solutions on the account of silicate minerals giving uranophane proved by spatial dissolving and replacement for quartz, perthite and plagioclase by uranophane. Presence of several processes of alteration (silicification, seiricitization, kaolinization and hematization) enhances the idea of post-magmatic effect of the hydrothermal solutions.

Three postulations may be proposed for the secondary syngenetic radioactive minerals; the first in the silica-poor magma where the uranous ions (U^{4+}) of uraninite combine with the other trace elements such as the lead and few silica forming Kasolite. The second in the silica-rich magma where the uranous ions (U^{4+}) combine completely with the silicate and crystallize as coffinite that transformed to uranophane ($Ca(UO_2)_2SiO_3(OH)_{2.5}(H_2O)$). The third postulation, where uranous ions (U^{4+}) of uraninite combine with the radiogenic lead to form kasolite; the magma progressively evolved and the uraninite evolved to coffinite and transformed to uranophane. Thus, the two secondary minerals are derived from- and genetically related to the primary uraninite of the magma proved by presence of kasolite (low silica) accompanying the uranophane (silica-rich). Hence, the postulation of evolved magma, is the most suitable for modeling of the mineralized granite in GII-occurrence stimulating the event of U-enrichment of G. Gattar.,

The epigenetic secondary uranium minerals comprising the minerals that formed post magmatic where the uranous ions (U^{4+}), derived from distal uranium-rich source, oxidized to uranyl ions (U^{6+}) that soluble in the hydrothermal solutions. They moved and reprecipitated when reduced in presence of reducing agent. The process of replacement is an epigenetic process where the hydrothermal minerals dissolve the essential minerals (feldspars and quartz) replacing them by iron oxides and secondary uranium minerals.

Acknowledgements

I would like to express my gratitude to my colleagues in NMA, Prof. Mohamed G. El-Feky for picking the samples and reviewing the manuscript and also to the members of ESEM Lab. especially Prof. Gehan Ali.

REFERENCES

Anjos, A.M.; Veiga, R.; Soares, T.; Santos, A.M.A.; Aguiar, J.G.; Frascá, M.H.B.O.; Brage, J.A.P.; Uzêda, D.; Mangia, L.; Facure, A.; Mosquera, B.; Carvalho, C., and Gomes, P.R.S., 2005. Natural radionuclide distribution in Brazilian commercial granites. Radiation Measurements, 39, 245-253.

Attawiya. M.Y.; Bishady, A.M.; Shalaby, M.H, and Darwish M.E., 1999. Mineralogical, geochemical and radioactivity studies on the G. Qattar granites and their episynetized varieties, North Eastern Desert, Egypt. 4th inter. Conf. Geochemistry, Alex. Univ., Egypt, 341-372.

Bau, M., 1996. Controls on the fractionation of isovalent trace elements in magmatic and aqueous systems: Evidence from Y/Ho, Zr/Hf and lanthanide tetrad effect. Contrib. Mineral. Petrol., 123, 323-333.

Belousova, E.A.; Greffin, W.L., and Pearson, N.J., 1998. Trace elements composition and cathodoluminescence properties of Southern African Kimberlitic zircons. Mineralogical Magazine, Australia, 62(3), 355-366

Boynton, W.V., 1984. Cosmochemistry of the rare earth elements: Meteorite studies. In: Rare Earth Element Geochemistry(Henderson, P.,Ed.). 63-114

Burns, P.C., and Finch, R., 1999. Uranium mineralogy, geochemistry and the environment. Reviews in Mineralogy, 38, 157p.

Cathelineau, M., and Holliger, P., 1987. Polyphase metallogenesis of hydrothermal uranium veins from the southern amoricon massif, France. Proc. Int. Mtg Nancy, 212-217.

Cebron, F.; Ildefonse, P., and Sichere, M.C., 1993. New mineralogical data on uranophane and ßuranophane: Synthesis of uranophane. Mineral. Mag., 57, 301-308.

Cuney, M., and Friedrich, M., 1987. Physicochemical and crystal-chemical controls on accessory mineral paragenesis in granitoids: Implications for uranium metallogenesis. Bulletin Mineralogie, 110, 235-247.

Darnely, A.G., and Ford, K.L., 1989. Regional airborne gamma-ray survey; a review. In: Proc. exploration 87: Third decennial international conference in geophysical and geochemical exploration for minerals and ground water. Geol Surv. Canada, 3, 960.

Darnely, A.G., 1982. Hot granite; some general remarks. In: Uranium in granites(Maurice, Y.T., Ed.). Geol. Surv. Canada, 81-23, 1-10.

Darwish, M.E.,1999. Geology, mineralogy, geochemistry and radioactivity of some episyenitized granites of Gabal Qattar, North Eastern Desert, Egypt. M.Sc.Thesis, Fac. Sci., Menoufia Univ., Egypt.

Doventon, J.H., and Prensky, S.E., 1992. Geological applications of wire line logs: A synopsis of developments and trends. Log. Anal., 33 (3), 286-303.

El-Kaliouby B.A.; El Sayed M.H., and Dawood Y.H., 2003. Geochemistry and uranium mineralization of the younger granite-Hammamat sediments contact zone, Gattar area, North Eastern Desert, Egypt. MERC Ain Shams Univ, Earth Sci Ser, 17, 1-23.

El-Kholy, D.M.; Khamis, H.A., and El-Sandouly, H.L., 2019. Geology and structural relationship between uranium occurrences in the northern part of Gabal Gattar, Northern Eastern Desert, Egypt. Nuclear Sciences Scientific J., 8a, 1-18.

El-Mezayen, A.M.; Heikal, M.A.; El-Feky, M.G.; Shahin, H.A.; Abu Zeid, I.K., and Lasheen, S.R., 2019. Petrology, geochemistry, radioactivity, and M-W type rare earth element tetrads of El-Sela altered granites, South Eastern Desert, Egypt. Acta Geochimica, 38, 95-119.

El-Rakaiby, M.L., and Shalaby, M.H., 1992. Geology of Gabal Gattar batholith, Central Eastern Desert, Egypt. Inter. J. Remote Sens., 13, 2337-2347.

El-Shazly, E.M., 1970. Evolution of granitic rocks in relation to major tectonics. West commemoration volume, University of Sagar, India, 569-581.

El-Kammar, A.M.; Salman, A.E.; Shalaby, M.H., and Mahdy, A.I., 2001. Geochemical and genetical constraints on rare metals mineralization at the central Eastern Desert of Egypt. Geochemical J., 35, 117-135,

Frondel, C., 1958. Systematic Mineralogy of Uranium and Thorium. U.S. Geol. Surv. Bull., Series 1064, 400p.

Gadd, M.G.; Layton-Matthews, D., and Peter, J.M., 2016. Non-hydrothermal origin of apatite in SEDEX mineralization and host rocks of the Howard's Pass district, Yukon, Canada. Am. Mineral., 101, 1061-1071.

Gramaccioli, C.M., and Segalstad, T.V., 1978. A uranium- and thorium-rich monazite from a south-alpine pegmatite at Piona, Italy. Am. Mineral., 63, 757-761.

Hazen, R.M.; Ewing, R.C., and Sverjensky, D.A., 2009. Evolution of uranium and thorium minerals. Am. Mineral., 94, 1293-1311.

Herrman, A.G., 1970. Yttrium and lanthanides. In: Handbook of Geochemistry (Wedepohl, K.H., Ed.). Springer-verlag, New York, 11/2, 39-57.

Ibrahim, H.I., and Darwish, M.E., 2012. Geology and geochemistry of the granitic rocks and associated dykes, East Gabal Nuqra, South Eastern Desert, Egypt. Chin. J. Geochem., 31, 376-389.

Ibrahim, M.E.; Saleh, G.M., and Abd El-Naby, H.H., 2001. Uranium mineralization in two mica granite of Gabal Ribdab area, South Eastern Desert, Egypt, App. Rad. Iso., 55, 861-872.

Irber, W., 1999. The lanthanide tetrad effect and its correlation with K/Rb, Eu/Eu□, Sr/Eu, Y/Ho, and Zr/Hf of evolving peraluminous granite suites. Geochimica et Cosmochimica Acta, 63(3-4), 489-508.

Khazback, A.E.; Shalaby, M.H., and Raslan, M.F., 1995. On the occurrence of some secondary uranium minerals and fluorite in Gabal Gattar locality, Eastern Desert, Egypt. Egypt. Mineral., 7, 47-63.

Korzeb, S.L.; Foord, E.E., and Lichte, F.E., 1997. The chemical evolution and paragenesis of uranium minerals from the Ruggles and Palermao granitic pegmatites, New Hampshire: Canadian Mineralogist, 35, 135-144.

Kraemer, D.; Tepe, N.; Pourret, O., and Bau, M., 2017. Negative cerium anomalies in manganese (hydr) oxide precipitates due to cerium oxidation in the presence of dissolved siderophores. Geochim. Cosmochim. Acta, 196, 197-208.

Macfarlane, P.A.; Whittemore, D.O.; Townsend, M.A.; Doventon, J.H.; Hamilton, V.J.; CoyleIII, W.G.; Wade, A.; Macpherson, G.L., and Black, R.D., 1989. The Dakota Aquifer Program Annual Report, FY89. Appendix B. Kansas Geological Survey, Open-FileRept.90-27. http://www.kgs.ukans.edu/Dakota/vol3/fy89/index.htm.

Mahdy, N.M.; Shalaby, M.H.; Helmy, H.M.; Osman, A.F.; El-Sawey, E.H., and Abu Zeid, E.K., 2014. Trace and REE element geochemistry of fluorite and its relation to uranium mineralizations, Gabal Gattar area, Northern Eastern Desert, Egypt. Arab J. Geosci., 7, 2573-2589.

Maksimovic, Z., and Pantó, G., 1996. Authigenic rare earth minerals in karst-bauxites and karstic nickel deposits. In: Rare Earth Minerals, Chemistry, Origin and Ore Deposits, First Edition (Jones, F.A.; Wall, F., and Williams, C.T., Eds.). Springer Science and Business Media, 257-259.

Masuda, A.; Kawakami, O.; Dohmoto, Y., and Takenaka, T., 1987. Lanthanide tetrad effects in nature: two mutually opposite types, W and M. Geochem. J., 21, 119-124.

Matolin, M., 1991. Construction and Use of Spectrometric Calibration Pads Laboratory G-ray Spectrometry, NMA, Egypt. A Report to the Government of the Arab Republic of Egypt. Project EGY/4/030-03. IAEA.

McLennan, S.M., 1994. Rare earth element geochemistry and the "tetrad" effect. Geochim. Cosmochim. Acta, 58, 2025-2033.

Möller, P.; Giese, U., and Dulski, P., 1994. Behaviour of REE in alteration processes of granites. In: Thermal und Mineralwassern des Schwarlzwadles. Zeischrift Fachsektion Hydrogeol, 3, 118-131.

Montel, J.M., 1986. Experimental determination of the solubility of Ce-monazite in SiO2-Al2O3-K2O-Na2O meets AT 800ºC, 2 kbar, under H2O- saturated conditions. Geology, 1, 659-662.

Nardi, L.V.S.; Formoso, M.L.L.; Jarvis, K.; Oliveira, l.; Bastos Neto, A.C. , and Fontana, E., 2012. REE, Y, Nb, U and Th contents and tetrad effect in zircon from a magmatic-hydrothermal F-rich system of Sn-rare metal-cryolite mineralized granites from the Pitinga Mine, Amazonia, Brazil. J. South American Earth Sciences, 33, 34-42.

Nash, J.T.; Granger, H.C., and Adams, S.S., 1981. Geology and concept of genesis of important types of uranium deposits. Econ. Geol., 75th Anniv., 63-116.

Naumov, G.B., 1959. Transportation of uranium in hydrothermal solution as carbonate. Geochemistry, 1, 5-20.

Nossier, L.M., 1996. U-F bearing episyenitized "desilicified" granitic rocks of Gabal Gattar, North Eastern Desert, Egypt. Egyptian Academy of Sciences, 46, 375-396.

Osmond, J.K.; Dabous A.A., and Dawood Y.H., 1999. U series age and origin of two secondary uranium deposits, Central Eastern Desert, Egypt. Economic Geol., 94, 273-280.

Qicong, L., and Congqiang, L., 2010. Geochemical behaviors of REE and other trace elements during the formation of strata bound Skarns and related deposits: A case study of the Dongguashan Cu (Au) Deposit, Anhui Province, China. Acta Geologica Sinica, 77 (2), 246-257.

Raslan, M.F., and El-Feky, M.G., 2012. Radioactivity and mineralogy of the altered granites of the Wadi Ghadir shear zone, South Eastern Desert, Egypt. Chin. J. Geochem., 31, 30-40.

Rismsaite, J., 1982. The leaching of radionuclides and other ions during alteration and replacement of accessory minerals in radioactive rocks. Paper Geol. Surv. Can., 82-1B, 253.

Roz, M.E., 1994. Geology and uranium mineralization of Gabal Gattar, North Eastern Desert, Egypt. Unpublished M.Sc. Thesis, Fac. Sci., Cairo Univ., Egypt, 175p.

Sallam, O.R.; El-Tohamy, A.M., and Abbas, A.A., 2020. Mineralogy and geochemistry of uraniferous sandstones in fault zone at Wadi El-Sahu area, Southwestern Sinai, Egypt: Implications for provenance, weathering and tectonic setting. Acta Geologica Sinica, (In press).

Salman, A.B.; El-Aassy, I.E., and Shalaby, M.H., 1986. New occurrence of uranium mineralization in Gabal Gattar, North Eastern Desert, Egypt. Ann. Geol. Surv. Egypt, XVI, 31-34.

Schurman, H.M., 1966. The Precambrian along the Gulf of Suez and the northern part of the Red Sea. E.J. Bill, Netherlands, 404p.

Schwinn, G., and Markl, G., 2005. REE systematics in hydrothermal fluorite. Chemical Geol., 216, 235-248.

Shalaby, M.H., 1996. Structural controls of uranium mineralization at Gabal Gattar, North Eastern Desert, Egypt. Egypt. Academy Sci., 46, 521-536.

Shalaby, M.H.; Abu Zeid, E.K. , and Mahdy, N.M., 2015. On the petrogenesis and evolution of U-rich granite: insights from mineral chemistry studies of Gattar granite, North Eastern Desert, Egypt. Arab J. Geosci., 8, 3565-3585.

Snelling, A.A., 1980. Uraninite and its alteration products, Koongarra uranium deposit. Poc. Int. Uranium Symposium on the Pine Greek Geosyncline, 487-498

Streckeisen, A., 1976. To each Plutonic rock its proper name. Earth Sci. Rev., 12, 1-33.

Tang, H.S.; Chen, Y.J.; Santosh, M.; Zhong, H., and Yange, T., 2013. REE geochemistry of carbonates from the Guanmenshan formation, Liaohe group, NE Sino-Korean craton: Implications for seawater compositional change during the great oxidation event. Precambrian Res., 227, 316-336.

Zhang, J.; Amakawa, H., and Nozaki, Y., 1994. The comparative behaviors of Yttrium and lanthanides in the seawaters of North Pacific. Geophysical Research Letters, 21, 2677-2690.

إشعاعية، نشأة والتأثير الرباعي للعناصر الأرضية النادرة لجرانيت جبل جتار المتمعدن،شمال الصحراء الشرقية، مصر

إيهاب قرني أبو زيد

يقع جبل جتار في الجزء الشمالي من الصحراء الشرقية بين خطي عرض ٥٢' ٢٦ ° ، ٠٨' ٢٧ ° شمالاً وخطي طول١٣' ٣٣ ° ، ٢٦' ٣٣ ° شرقاً ويحده من الركن الشمال الشرقي صخورالديورايت والجرانوديورايت ومن الركن الشمال الغربي رواسب الحمامات حيث يمتد بينهما وادي بلي. وتتميز منطقه الدراسة بوجود التراكيب الجيولوجية المعقدة ومناطق القص حيث تتركز معادن اليورانيوم.

أوضحت الدراسة البتروجرافية لمنطقة البحث (GII) أنها تتكون من صخور السيانوجرانيت ثنائي الفلسبار عالي الكوارتز والحاوي للمسكوفيت مع وجود العديد من عمليات التحول المعدني. أوضح الفحص الميكروسكوبي وجود نوعين من معادن اليورانيوم الثانوية بالإضافة إلي معادن اليورانيوم الأوليه. النوع الأول من معادن اليورانيوم الثانوية يشمل معادن اليورانوفين والكازوليت التي تكونت في صهير مشتق من المعادن الأولية وهي دائماً ما تكون مصاحبة لمعادن الزرقون، الفلوريت والجالينا. أما النوع الثاني فيشمل اليورانوفين الفوق صهيري والذي تكون بفعل المحاليل الحارة والإغتناء بعنصر اليورانيوم المنقول من مصدر آخر.

أوضحت الدراسة الإشعاعية للمنطقة إرتفاع المستوي الإشعاعي للجرانيت حيث يصل محتوي اليورانيوم إلي ٤٦٠٠ جزء من المليون بينما إنخفض محتوي الثوريوم بحيث لا يتعدي ٩٠٠ جزء من المليون وأن متوسط نسبة الثوريوم/يورانيوم هو ٠,٠٣ وهي نسبة أقل من النسبه العالمية وتدل على الإغتناء باليورانيوم بواسطة المحاليل الحارة. أوضحت العلاقات الثنائية بين اليورانيوم والثوريوم أنها علاقة طردية بينما أوضحت العلاقات الأخري التوزيع العشوائي مما يدل علي إرتباط الإشعاعية المرتفعة في المنطقة بالمحاليل المائية الحارة والتي أعادت توزيع تلك العناصر المشعة من جديد محدثة عملية اثراء لليورانيوم.

بدراسة المعادن المشعة بواسطة الميكروسكوب الماسح الإلكتروني أمكن تأكيد وجود معادن اليورانيوم الأولية (اليورانينيت والبيتشبلند) بالإضافه لمعادن اليورانيوم الثانوية (اليورانوفين والكازوليت) ومعدن الجالينا كمصدر رئيسي لعنصر الرصاص.
تمت دراسة محتوي العناصر الأرضية النادرة لعينات مختارة من المنطقة، وتبين أن محتوي العناصرالخفيفة أكثرمن محتوي العناصرالثقيلة وأنها ذات تأثير رباعي من النوع (M) مما يوضح أن هذا الجرانيت تطورخلال المرحلة الأخيرة من الصهير و أنه تأثر بالمحاليل الحارة اللاحقة للصهير.